Beeswax multifunctional composites with thermal-healing capability and recyclability

Ricardo Brito-Pereira[1,2], Clarisse Ribeiro[1], Carmen R. Tubio[3], Nelson Castro[3], Pedro Costa[1,4,*], Senentxu Lanceros-Mendez[3,5]

1- Center of Physics, University of Minho, 4710-058 Braga, Portugal
e-mail: pcosta@fisica.uminho.pt;
2- CMEMS-UMinho Research Unit, University of Minho, 4800-058 Guimarães, Portugal
3- BCMaterials, Basque Center for Materials, Applications and Nanostructures, UPV/EHU Science Park, 48940 Leioa, Spain.
4- Institute for Polymers and Composites IPC, University of Minho, 4800-058 Guimarães, Portugal
5- Ikerbasque, Basque Foundation for Science, 48009 Bilbao, Spain

Keywords: Natural beeswax; graphene; biocompatible composites; functional composite; thermal-healing material

Abstract

Natural beeswax reinforced with conductive nanofillers allows solvent-free processing and presents remarkable functional responses as piezoresistive and thermoresistive sensors with thermal healing capability. The low melting temperature of the composites, around 60 ºC, allows additive manufacturing of conductive patterns with high electrical conductivity of 50 S/m. Further, the graphene/beeswax composites show suitable deformation and temperature sensing characteristics based on the piezoresistive and thermoresistive sensibilities, around GF≈9 and S≈ 120%/ºC, respectively. Natural beeswax is a food and drug administration approved substance, and all graphene/beeswax composites present no cytotoxic behavior, demonstrating their potential use for biomedical applications.

Proof-of-concept demonstrate the conductive and thermal-healing properties of the screen-printed sensors developed both on paper and Kapton substrates, proving the applicability and multifunctionality of the developed materials. Finally, the multifunctional composites can be recycled and reused without losing their electrical and functional performances.

1. Introduction

Polymer composites can be developed with tailorable properties and functional responses to be applied in an increasing range of applications. Further, they can be processed by additive manufacturing, improving device integration and reducing the environmental impact of both materials and processes [1]. Mechanical flexibility, chemical resistance, easy and low-cost processability of polymer composites have attracted attention for application in a variety of areas including energy harvesting and storage [2], biomedicine [3], electronic devices [4] or sensors [5, 6], among others. Most of the commonly developed high-performance polymers and polymer composites are of synthetic nature and present environmental concerns to processing and recyclability, including environmental toxicity issues. Nevertheless, non-biodegradable or petroleum-based polymers overwhelm our daily life and economy and critically lead to both increased crude oil dependence and increased materials waste with the corresponding environmental impact [7]. In fact, the polymer waste in the ocean will grow up to 150 million tons by 2025 [8] and biodegradable materials can save emissions equivalent to 250-300 million tons of carbon dioxide annually [9].

In particular, the current transformation driven by the digitalization of society and economy through the Industry 4.0 and Internet of Things (IoT) paradigms will lead to a strong increase or sensors and interconnected devices [10]. Electronic waste (e-waste) is thus a critical problem to be addressed as it will increase in the next decades with the exponential increase of manufactured materials, reaching nearly 100 million tons of e-waste by 2050 [10]. To date, only one-fifth of e-waste materials are collected and recycled and different countries are implemented regulations to control their pollution [11]. Thus, the next generation of electronic materials and, in particular, sensing materials (environmental, pH, motion, force, temperature, among others) must be based on recyclable and/or reusable materials.

Due to increasing environmental concerns, society requires the implementation of technologies based on a new generation of materials compatible with sustainable environment policies (European Strategy for Plastics in a Circular Economy [12], or USA Presidential Executive Order 14057 in 2021 [13]) without diminishing the functional properties in nowadays existing solutions, mostly based on petroleum polymers [14]. The challenge is thus replacing nonrenewable synthetic materials for natural origin ones with low-cost, bio-renewable characteristics and environmentally friendly processing techniques, contributing to sustainable development [15].

In this context, natural or biopolymers have been increasingly investigated in recent years. Natural polymers can be categorized into different classes: renewable resources/biomass, from animal or plant origin, and biodegradable synthetic polymers such as polylactic acid (PLA) or polyhydroxybutyrate (PHB) [16, 17]. The most common natural biopolymers of animal origin are chitosan, gelatin and beeswax, together with some natural proteins, such as keratin and silk [18]. Beeswax is a food and drug administration (FDA) approved substance [19] and is largely used in food packaging and coating applications, with excellent vapor barrier and grease resistance [20] that can be blended or reinforced with other biopolymers/fillers to modulate and/or introduce specific properties [17]. The beeswax's low-melting temperature combined with its processability by additive manufacturing makes it suitable for different applications including sensors and phase changing materials [21]. In fact, the use of natural wax in added-value products also supports increasing the economic impact and the preservation of bees-products and natural habitats, maintaining the honeybee colonies sustained and away from pesticide-rich environments [22].

One of the most interesting functional modifications of materials, such as wax, is by developing electrically conductive composites through the addition of conductive fillers, and opening applications in the area of printed electronics [23], among others. Graphene is one of the most used conductive nanofiller for the development of conductive composites, based on its electrical conductivity, 2D structure, interaction with biomolecules and successfully being used in biomedical applications [24]. The intrinsic conductivity of graphene is similar to carbon nanotubes (1D materials) [25], being the graphene easier to disperse and exhibiting cytocompatibility up to high filler content [26]. Synthetic wax reinforced with conductive fillers [27] has been developed as a functional material [28] by additive manufacturing, as the low-melting temperature of wax becomes practical to be processed by molding (3D) [28] or by printing techniques, such as screen-printing [28, 29] or doctor blade. Moreover, wax matrices can be processed without the use of any solvents or by using greener solvents (water or ethanol) to deagglomerate the carbon nanofillers and increase filler dispersion in wax matrices [28].

This work demonstrates the potential of conductive natural beeswax to be used for next-generation printable electronics. Deformation and thermal sensors are achieved based on graphene in beeswax composites processable by screen-printing on different substrates such as Kapton and paper and by 3D molding. In addition, the low-melting temperature is taken to advantage for the implementation of thermal healing of the functional response

in the developed systems. Further, it is demonstrated that the composites can be recycled and reused.

2. Experimental Section

2.1. Materials

Natural beeswax (ISO 16128) was purchased from Alexmo, Germany. The beeswax presents yellow color, a melting temperature between 62 to 65 ºC and a density of 0.97 g/cm^3. As conductive fillers, high-quality graphene nanoplatelets obtained by physical processing were used (Graphenest, Portugal). The graphene is composed by 2-30 layers with <10 nm of thickness and 1-20 μm of particle size. As substrates, Kapton was purchased from DuPont, USA, and paper was purchased from Navigator Company, Portugal. All materials were used as received from the providers.

2.2.Preparation of the conductive wax composites

For the preparation of the graphene/beeswax (G/BW) composites, illustrated in Figure 1, graphene was first added in the proper filler content (0, 5, 10, 20 weight percentage (wt.%)) to 1.5 g of beeswax, placed at 75 °C on a hotplate (Präzitherm, model PZ23-2) and mechanically mixed for 1h at 100 rpm (*Heldolph D-91 126*) to achieve a well-dispersed mixture. The nomenclature of the samples along the work will be the following: filler content/matrix as, for example, 5G/BW represents the 5 wt.% graphene content reinforcing beeswax composites.

The materials were then processed by two different techniques: 3D molding and 2D screen-printing.

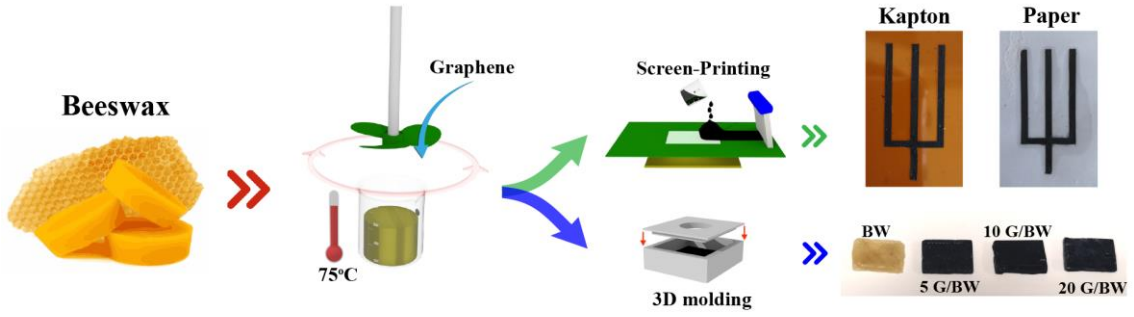

Figure 1- Processing steps for the fabrication of the graphene/beeswax composites by screen-printing and molding.

2.3. 3D Molding

3D wax and wax composites were deposited in a previously 3D printed (*Prusa* i3 MK3S+) polyvinyl alcohol (PVA) (*Prusa* Prima SELECT PVA+, 1.75 mm) cubic mold with the inner dimensions of 1 cm^3 (10×10×10 mm), allowing to obtain samples with the specific 3D structure. Beeswax and composites were heated at 75 ºC in a hotplate and the mold was filled. The PVA mold structure was then completely dissolved in water at room temperature for 12 h.

2.4. Screen-printing

Composites with different filler concentrations were also processed by screen-printing at 75 ºC (above wax melting temperature) in specific designs, including lines (50×2 mm of lenght×width) and complex interconnected system (fork type with 2 mm width lines and 10 mm distance between them). Commercial Kapton (DuPont, 125 μm thickness) and common office paper (Navigator 80 g/m^2) was used as a flexible substrate, fixed in a hotplate at 75 °C during the printing process.

For the screen-printing of the samples, the screen (200 mesh of nylon on an aluminum frame) was placed at 1 mm distance from the hotplate surface and the previously melted wax-based ink was pressed with the screen stencil through the mesh to print (one single pass of stencil) the specific patterns (50×30 mm lines with 50± 10 μm thickness and tri-fork shapes) over the Kapton and paper surface. The printed design was ready for use after removing it from the hot plate and allowing it to cool down to room temperature, with no further treatment.

2.5. Samples Characterization

Morphological evaluation was carried out by scanning electron microscopy (SEM) in order to assess the surface morphology of the samples and the dispersion of graphene nanofillers within the beeswax matrix. The cross section and surface images of the composites were obtained using a NanoSEM-FEI Nova 200 (FEG/SEM) at magnifications of 1 000× and 15 000×.

The surface wettability of the different samples was evaluated at room temperature measuring the contact angle of 3 μL ultrapure water drops, using a Data-Physics Contact Angle System OCA 15EC and the SCA20 software. The contact angle of each sample was calculated and presented as the average and standard deviation of six measurements, which were performed on the surface of the materials at different sample locations.

Fourier transformed infrared (FTIR) spectroscopy was used to evaluate the characteristics vibration bands of the composites, using a Jasco FT/IR-4100 in the attenuated total reflectance (ATR) mode. FTIR-ATR spectra were obtained between 4000 and 600 cm^{-1}, using 64 scans at 4 cm^{-1} resolution.

Thermal analysis was carried out by differential scanning calorimetry (DSC) from 30 to 250 °C at a heating rate of 20 °C/min using a model DSC200 F3 Maia (NETZSCH) under a dry nitrogen atmosphere.

The volume electrical conductivity of the samples was determined using screen-printed 50 ± 10 μm thick samples and molded 3D samples using 5 mm diameter gold electrodes deposited on both sides of the samples with a Polaron SC502 sputter coater. The electrical conductivity was determined by the characteristic I-V curves in the voltage range between -10 V to +10 V at laboratory conditions with a Keithley 6487 picoammeter/voltage source. The electrical conductivity (σ) was determined considering the geometrical factors of the samples according to:

$$\sigma = \frac{l}{R.A} \tag{1}$$

where R is the electrical resistance, l is the sample thickness and A is the area of the electrodes.

Piezoresistive tests were carried out in the *4-point-bending* mode using a universal testing machine Shimadzu model AG-IS with a 500 N load cell, measuring the electrical resistance variation under mechanical deformation with a multimeter model Agilent 34401A. The *4-point-bending* mode (Figure 4A) was applied to samples with dimensions 30 mm×10 mm and 50 μm of thickness manufactured by screen-printing on Kapton and paper substrates. The printed composite was glued (transparent double-sided adhesive tape from Tesa) to a flexible polypropylene (PP) substrate with a thickness of 1 mm. The electrodes on the composite surface were printed using silver ink (Agar Scientific, AGG3790) with an area of 20×10 mm (length×width). The piezoresistive response was evaluated for the 20G/BW sample for 1, 3 and 5 mm of bending at a 3 mm/min strain speed.

The piezoresistive response sensitivity (gauge factor, GF) of the composite was calculated after equations 2 and 3 [30, 31]:

$$GF = \frac{\Delta R/R_0}{\Delta l/l_0} = \frac{\partial \rho/\rho_0}{\varepsilon} + 1 + 2\upsilon \tag{2}$$

where ΔR is the electrical resistance variation, R_0 is the initial value of the resistance. The Poisson coefficient is represented by υ (υ=0.37 [32]), l is the mechanical displacement, ρ the electrical resistivity and $\varepsilon = {}^{\Delta l}/_{l_0}$ the strain. For the *4-point-bending* mode experiments, the strain was calculated from the theory of pure bending, valid between the inner loading points and given by [30, 33].

$$\varepsilon = \frac{3dz}{5a^2} \quad (3)$$

where d≈ 1.1 mm is the thickness of the glued sample plus the support, the vertical displacement, z, is 1, 3 and 5 mm, and the distance between bending points, a=15 mm, are represented in Figure 4A.

The piezoresistive response (equation 2) is determined by two contributions: the geometrical effect (1+2υ= 1.74 [32]) and the intrinsic component that depends on the electrical conductivity variation due to the graphene nanofillers network rearrangements [5].

The thermoresistive response was evaluated in two different temperatures ranges: from 25 to 50 ºC at 5 ºC/min heating rate and from 35 to 40 ºC at 1 ºC/min heating rate for screen-printed samples on Kapton and paper substrates. The 20G/BW composite samples were cut in rectangular shapes with 10 mm×10 mm of width×length and two silver rectangular electrodes (Agar scientific, AGG3790) were printed at 5 mm of distance and 10 mm of length among them on top side of the sample. Copper thin wires were glued to the silver electrodes to connect the multimeter Agilent 34401A and collect the electrical resistance data. The thermoresistive evaluation was carried out by measuring the electrical resistance variation under heating of the samples in a Linkam THMSE 600 temperature oven. The thermoresistive sensitivity (*S*) was calculated after equation 4 [34]:

$$S = \frac{{}^{\Delta R}/_{R_0}}{\Delta T} \times 100 \quad (4)$$

Thermal healing evaluation was performed on screen-printed composites with 20 wt.% graphene content (20G/BW) using a Linkam model THMSE 600 at 60 ºC for 5 min for each different material. The samples were printed in a tri-forked-shape with previously dimensions. Different fork tines were cut using a sharp scalpel to interrupt the drawn line. Then, the samples were placed in the oven heated at steps of 10 min at 50, 60 and 70 ºC, measuring simultaneously the electrical resistance with a multimeter Agilent 34401A.

2.6. Cytotoxicity assay

The indirect cytotoxicity of the different samples was evaluated through the ISO 10993-5 standard test method. For that, L929 cells were cultured in 75 cm^2 cell culture flask, at 37 °C, in a humidified environment with 5% CO_2, using Dulbecco's modified Eagle's medium (DMEM, Biochrom) containing 4.5 g/L glucose, 10% fetal bovine serum (FBS, Biochrom) and 1% (v/v) penicillin/streptomycin solution (P/S, Biochrom).

Before the assay, the samples were cut with approximately 1.5 cm^2 and sterilized. For the sterilization, the samples were submitted to ultraviolet radiation for 1 h on each side and after that washed with a sterile phosphate-buffered saline solution (PBS, pH 7.4).

Then, the sterilized samples were incubated in DMEM in a 24-well tissue culture plate for 24 h. At the same time, a suspension of 5×10^4 cell/mL was seeded in 96-well tissue culture plate and incubated for 24 h to ensure cell attachment. After 24 h, the cell culture medium in the 96-well culture plate was removed and replaced with 100 µL of the culture medium previously in contact with each different sample (as-prepared DMEM). In this experiment, it was also utilized a negative control (DMEM) and a positive control (dimethylsulfoxide (DMSO) at 20%). Then, the 96-well culture plate was incubated for 72 h and then, the cell metabolic activity of each well was quantified with (3-(4,5-dimethylthiazol-2-yl)-5-(3-carboxymethoxyphenyl)-2-(4-sulfophenyl)-2H-tetrazolium) (MTS, Promega). Briefly, the cell culture medium of every well was removed, and fresh medium containing MTS solution (in a 1:5 ratio) was added to each well and incubated for 2 h. Afterwards, the optical density was measured at 490 nm using a spectrophotometric plate reader (Biotech Synergy HT). The cell viability was calculated according to equation 5.

$$Cell\ viability\ (\%) = \frac{\text{absorbance of sample}}{\text{negative control absorbance (DMEM)}} \times 100 \qquad (5)$$

3. Results and Discussion

Natural wax and composites reinforced with graphene were morphologically characterized to evaluate the dispersion of the fillers within the polymer matrix. Representative scanning electron microscopy, SEM, cross section images are presented in Figure 2 for the 3D molded samples (Figure 2A to F): for beeswax (Figure 2A and B),

10G/BW (Figure 2C and D) and 20G/BW (Figure 2E and F) composites. Further, surface SEM images of the screen-printed patterns over paper (Figure 2G) and Kapton (Figure 2H) are also shown. In all cases, the samples are characterized by a homogeneous and continuous structure without holes or voids, for both preparation methods. The graphene dispersion is similar for composites with 10 or 20 wt.% contents, presenting also similar overall microstructure. Further, molded and screen-printed samples present low surface roughness with relatively flat morphology [35, 36]. Comparing both processing methods, screen-printed samples present a lower rugosity than 3D molded samples, which is related to the characteristic roughness of the poly(vinyl alcohol), PVA, 3D-printed molds, which is transferred to the surface characteristics of the composite in the solidification process. By comparing the 20G/BW samples prepared by screen-printing (Figure 2G and H), the printed sample over Kapton (Figure 2H) is the composite with the lowest rugosity, due to the smooth substrate microstructure of the polymer compared to paper. Further, synthetic and natural waxes show excellent adhesion properties, leading to coating applications with UV protection characteristics, among others [37].

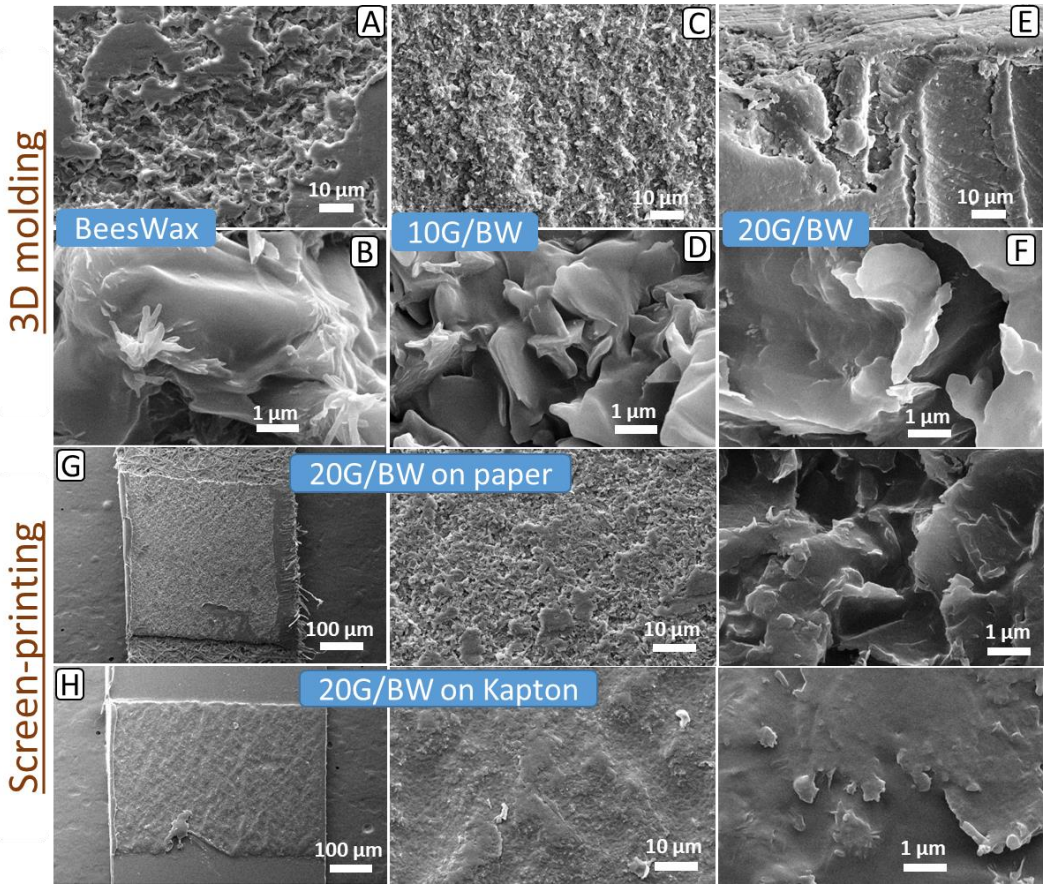

Figure 2- Cross section SEM images showing the morphological characteristics of beeswax (A and B) and composites with 10 (C and D) and 20 wt.% graphene (E and F). Surface SEM images of the 20G/BW composite screen-printed over paper (G) and Kapton (H). 50×, 500× and 10 000× magnifications are presented.

Beeswax presents low viscosity, which allows simple processing and obtaining homogeneous films. Reinforcement graphene sheets are not clearly observed, even for higher magnification or larger filler contents, demonstrating that the wax completely involves the graphene sheets during the preparation methods. As no agglomerates are observed, it can be concluded that the dispersion is effective in the wax composites.

Related to the surface characteristics of the samples, as all materials show the same surface chemistry, the water contact angle is 110º for beeswax and slightly decreases to near 100º for the 20G/BW composite (Figure 3A). The contact angle values are close between the samples printed over Kapton and 3D molded composites, based on the similar surface roughness (Figure 3E and H). Regarding the composite samples screen-printed on paper substrates the contact angle value is the highest, which is explained by

the absorption of wax along the thickness of the paper, which turns the surface rougher compared to other substrates [38]. All developed materials present high hydrophobicity, between 100º to 120º, which is characteristic of natural beeswax [39].

Infrared spectroscopy was performed to evaluate the characteristic vibrational bands of beeswax and the corresponding graphene composites (Figure 3B). Beeswax is mainly composed of esters fatty acids and long-chain alcohol where the functional groups −OH, C−O (H) and C=O are identified by infrared spectroscopy [40, 41]. The vibration bands at 2916 cm^{-1} and 2848 cm^{-1} are related to the elongating of CH_2 and CH_3, respectively [42] and at 1733 cm^{-1} it is observed the lipid absorption from the C=O group of cholesterol ester. The CH_2 bending and CH_3 asymmetric deformations are present at 1462 cm^{-1} and 1375 cm^{-1}, and the CH_2 rocking vibration is present at 718 cm^{-1} [43]. Among different wax types, including natural and synthetic types, the footprint of beeswax is the C=O (stretching vibrations), CH_2 (scissors deformation) and C-H (bending vibrations) corresponding to the esters and hydrocarbons compounds of beeswax [40]. The graphene content embedded in the beeswax does not change any of the characteristic absorption bands of natural wax [42], demonstrating that there is no chemical bonding between the matrix and the filler.

The thermal characteristics of the beeswax and the corresponding composites are analyzed from the DSC thermograms presented in Figure 3C, where natural beeswax is characterized by a single melting transition around 60 ºC [40, 42]. The melting temperature of beeswax seems to slightly increase with the incorporation of graphene up to 2 ºC, being nearly independent of the filler content. This effect is mainly attributed to interface effects and the difference in thermal conductivity between the graphene and the polymer [42].

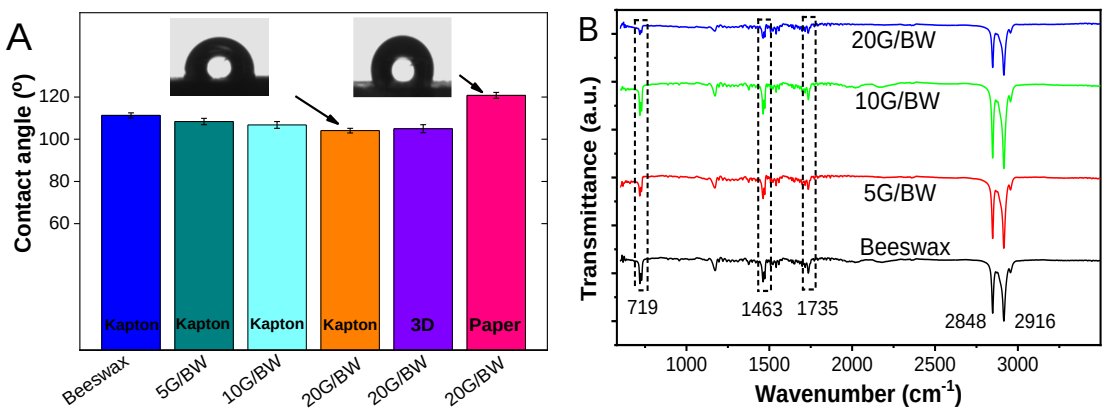

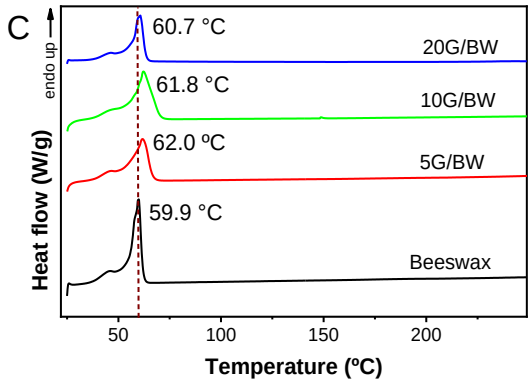

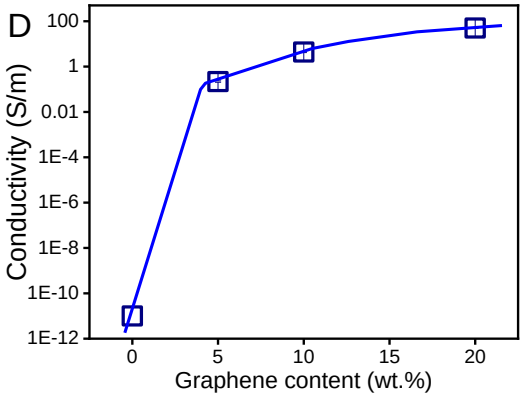

E Natural Polymer	Filler Type	Electrical Conductivity (S/m)
Rubber	CB/CNT	0.79 [44]
	GNP/PANI	0.05 [45]
	CB	10 [46]
Cellulose	GO	71.8 [47]
Silk Fibroin	CNT	0.0012 [48]
Beeswax	**G**	**50, this work**

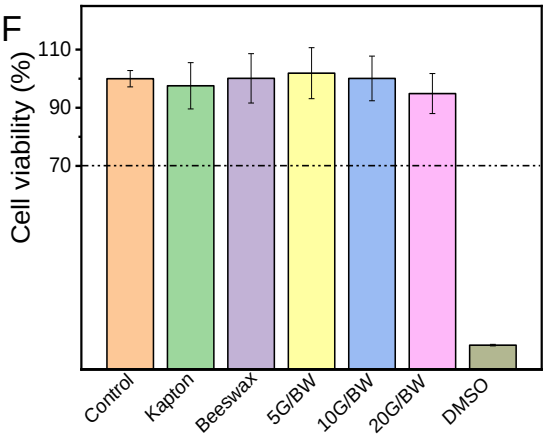

Figure 3- A) Water contact angle, B) FTIR spectra and C) DSC thermograms for beeswax and the corresponding graphene composites with 5, 10 and 20 wt.% filler content. D) Electrical conductivity of the materials and E) comparison with related natural polymer composites. F) Cytotoxicity assays of L929 cells in contact with the as-prepared extraction media exposed to the different materials for 72 h [relative cell viability is presented as the percentage of the negative control (n=4±standard deviation)].

A significant step to achieve multifunctional beeswax is due to the outstanding electrical properties of the composites. Figure 3D shows the electrical conductivity of the composites with increasing filler content, showing the percolative transition from insulator for pristine natural beeswax samples to electrically conductive composites. For 5 wt.% graphene content, the electrical conductivity increases 10 orders of magnitude with respect to pristine beeswax, the electrical conductivity reaching a value of 50 S/m for the 20G/BW composite. Thus, a conductive natural-based composite is achieved from low graphene content, with a percolation threshold lower than 5 wt.% filler content in composites with environmental-friendly low temperature processing without the use of solvents. In fact, the obtained results are among the best for natural polymer-based composites reinforced with conductive nanofillers, as indicated in Figure 3E, despite the

simple and low-cost processing techniques and materials. Furthermore, these composites can be processed by additive manufacturing and show excellent functional properties, as will be demonstrated in the following.

The cell viability of natural beeswax and the composites, which is a relevant feature for materials to be applied in the biomedical field, is presented in Figure 3F. Carbon nanostructures are used in medical research [49], but it has been reported that the use of graphene *in vivo* can lead to the premature death of cells [49]. The developed composites present cell viability values higher than 70% which is the threshold defined by the ISO standard 10993-5 to consider a material no cytotoxic. This leads to conclude that graphene sheets are effectively embedded inside the beeswax matrix, which preserves the high levels of biocompatibility. Furthermore, the cell morphology was also evaluated, and no differences were observed between the different samples and the normal media (DMEM). Cell viability opens the range of applications to the biomedical area, including sensors applied to wearables in sports or biomedical monitoring [50].

3.1. Piezoresistive and thermoresistive sensitivity of beeswax composites

The printed beeswax composites with the highest filler content, 20G/BW, were evaluated as functional materials for piezoresistive bending and thermoresistive sensing. For piezoresistive evaluation (Figure 4A), the material was subjected to different deformations of 1, 3 and 5 mm for 10 cycles (Figure 4B) and 500 cycles to observe the functional stability of the materials (Figure 4C) in *4-point-bending* mode. Figure 4B shows the electrical resistance variation (black lines, $\Delta R/R_0$) of the samples for the different strain variations (blue lines, represented just for the 5 mm maximum deformation), showing the proper response of the material under applied and released deformation. It is observed that the relative resistance variation increases with increasing deformation ($\Delta R/R_0 \approx$ 0.05, 0.2 and 0.3 for 1-, 3- and 5-mm bending, respectively) leading to larger *GF* with increasing applied deformation to the sensing material.

For the screen-printed 20G/BW sample over paper substrates, the cyclic stability was evaluated for 500 cycles under 5 mm bending (Figure 4C), being observed that the electrical resistance of the composite decreases over cycling, mainly for the first 50-60 cycles, tending then to stabilize the minimum and maximum values of the electrical resistance, as shown in the insets. The decrease for the first cycles are also observed for samples printed over Kapton and are attributed to irreversible reconfigurations of the

conductive network and stress relaxation that stabilize over cycling, a reported in the literature for related piezoresistive polymer composites [28, 51].

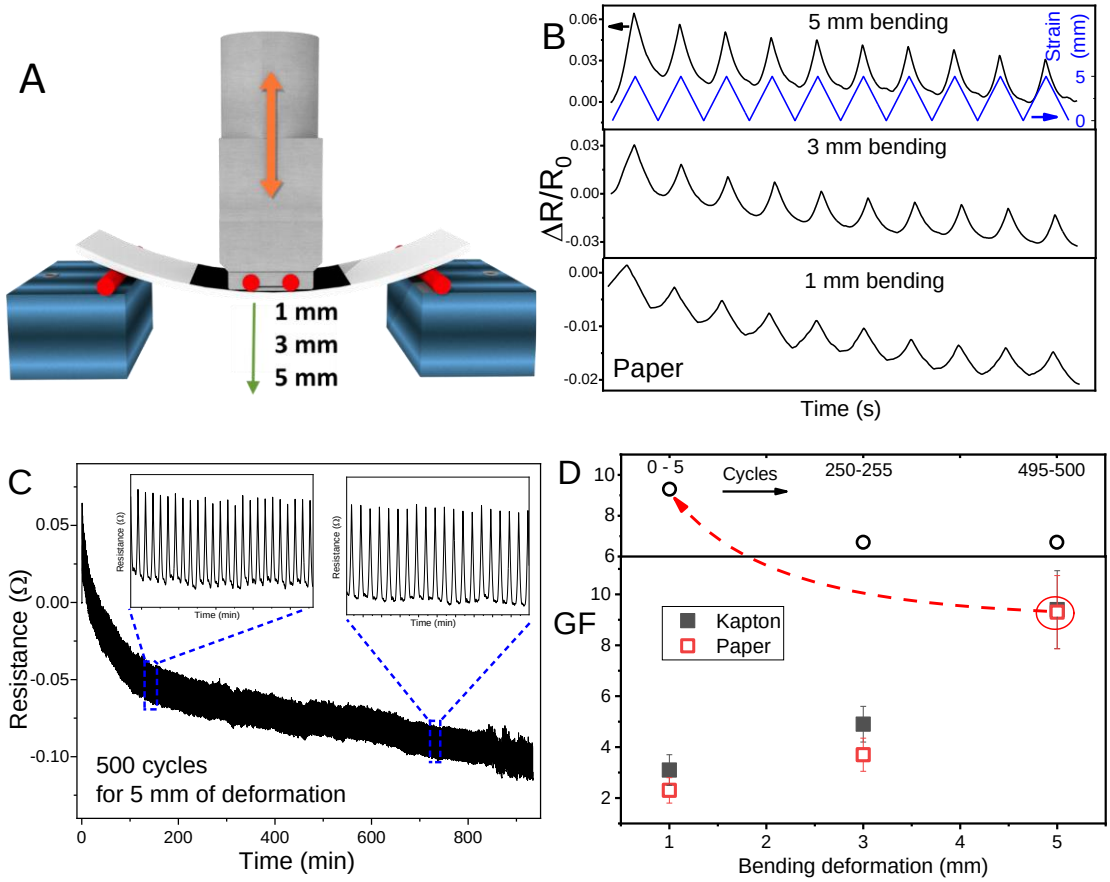

Figure 4- A) Schematic illustration of the piezoresistive measurements for the 20G/BW composites screen-printed over Kapton and paper substrates. Bending tests performed at B) 1-, 3- and 5-mm maximum deformations on paper substrate and C) 500 cycles at 5 mm of bending. D) Gauge factor for the screen-printed composites as a function of the maximum bending.

The piezoresistive response of the screen-printed samples on both Kapton and paper was quantified by the *GF* that was calculated after equation 2 (Figure 4B to D). The piezoresistive sensitivity increases with applied strain from $GF \approx 2$ to $GF \approx 10$ for bending of 1 and 5 mm, respectively, showing a non-linear response of the piezoresistive response. As the geometrical contribution to the *GF* is similar for all samples and equal to $1+2\upsilon = 2$ for perfect elastic material with $\upsilon = 0.5$ [5], the rearrangement of the graphene conductive network being, therefore, is a relevant contribution to the piezoresistive response, in particular for the larger deformations. In this way, the piezoresistive response is the result

of the geometrical and the intrinsic piezoresistive contributions, the latter being based on the increased distance between the graphene rearrangements under deformation, leading to variations in the tunneling effect between the graphene sheets embedded into the beeswax matrix [49]. When the space between graphene sheets is small enough, a tunneling effect occurs between individual sheets, leading to the formation of a local conductive network [49]. The external stimulus leads to changes in the geometry of the composite and the geometrical variations lead to increases/decreases in the tunneling current and, therefore, the electrical resistance of the composite [49]. In fact, Figure 4D shows that the *GF* increases from about 2 to 3 and then near 10 for 1-, 3- and 5-mm maximum bending, respectively, demonstrating that the intrinsic rearrangements of the graphene conductive network critically influence the performance of the sensor materials. Comparing reinforcing conductive nanofillers, graphene has a large potential for sensing applications as it allows high conductivity at low percolation thresholds [52].

The developed composites combine natural material with nanofillers and are processed by additive manufacturing as functional piezoresistive bending sensors, with excellent piezoresistive sensitivity and adequate mechanical properties. The piezoresistive response up to 5 mm maximum bending is favorably compared with stretchable porous paper sensors with CNTs or silver nanowires [53] where the GF is lower than 8 up to 100% of strain, natural rubber/cellulose reinforced with graphite, with GFs lower than 10 up to 30% of strain [54], or cellulose/graphene sensors with GF≈ 4 [55]. Synthetic polymer matrixes reinforced with conductive fillers present in general higher sensitivity and improved mechanical properties [56, 57], but they typically make use of toxic and harmful solvents in the processing, their recycling being also a critical issue [58].

To further explore the functionality of the developed beeswax-based composites, the thermoresistive response of the composite reinforced with 20 wt.% of graphene has been measured in the temperature range from 25 to 50 ºC (Figure 5A) and 35 to 40 ºC (Figure 5B), compatible with applications around body temperature.

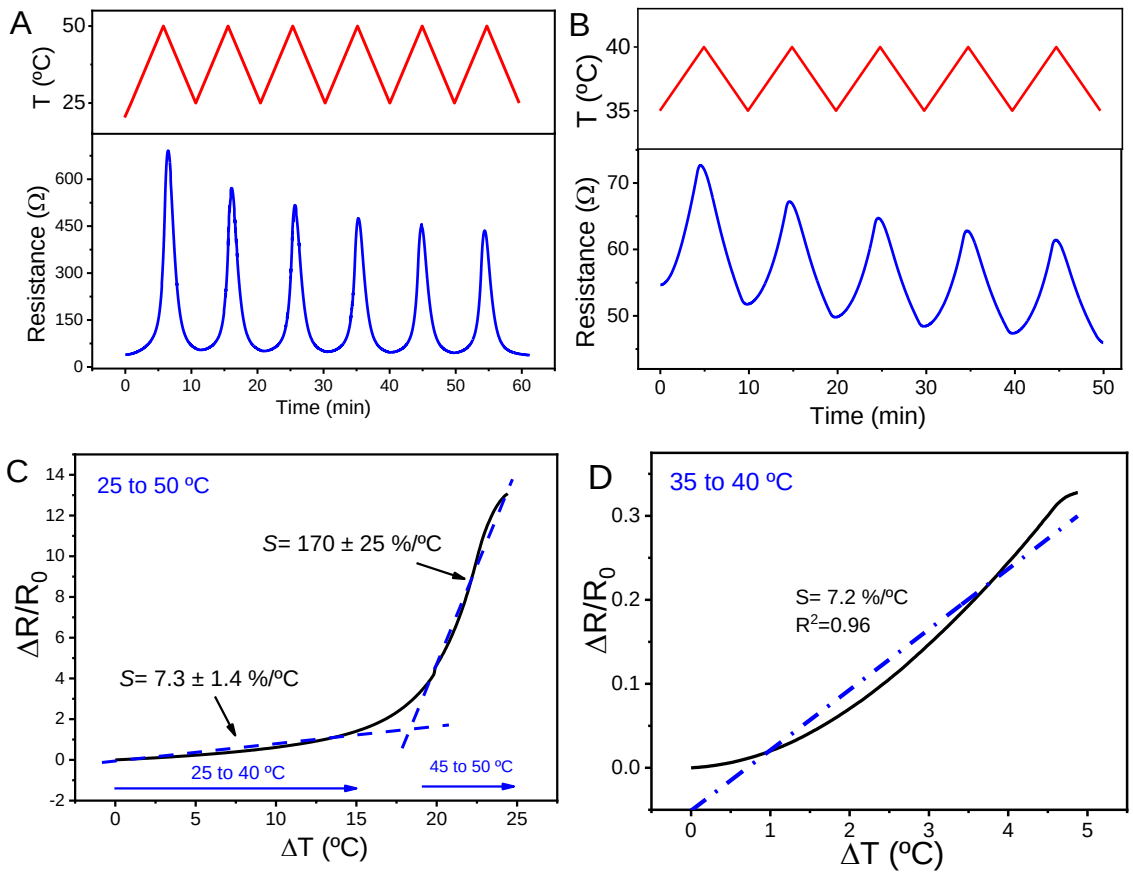

Figure 5- Thermoresistive response of the 20G/BW composites in the temperature range A) 25 to 50 ºC and B) 35 to 40 ºC. C) Sensitivity of the materials in two regions: from 25 to 40 ºC and from 45 to 50 ºC and D) linearity for temperature variations around human body temperature.

The thermoresistive sensitivity, *S*, determined using equation 4 is about 7.3 ± 1.4 %/ºC and 170 % ± 25%/ºC in the 25 to 40 ºC and from 45 to 50 ºC, respectively (Figure 5C). The linear region up to 40 ºC makes it possible to use these materials in applications to measure human body temperature variations or related applications (*S*= 7.2 %/ºC), as shown in Figure 5D. The low initial resistance of the samples, combined with the thermal sensing properties makes these natural-based composites high-performance thermoresistive materials. Graphene reinforced stretchable matrixes have been reported with a sensibility of 21.4%/ºC [59] but most polymer-based composites present values lower than 1%/ºC [34, 60], similar to pristine conductive fillers [34]. Thus, by using low melting temperature natural beeswax reinforced with conductive graphene, the thermoresistive sensitivity is up to 2 orders of magnitude higher than most related polymer-based composites.

3.2. Multifunctional sensing: proof-of-concept

The outstanding properties of the 20G/BW composite samples were explored as simultaneous temperature and force sensing functional materials processed by different additive manufacturing techniques. Piezoresistive force sensors were based on beeswax composite columns with 5×5 mm of area and 15 mm of height and a distance of 10 mm between them (Figure 6A), manufactured by molding using a PVA 3D-printed structure which was latter dissolved in water for 12h at 25 ºC. Further, thermoresistive measurements were based on screen-printed 20G/BW composite patterns with 50 μm of thickness and an area of 30×20 cm on a commercial Kapton film. Silver electrodes were screen-printed on both sensors, using a commercial silver ink.

The electrical resistance variation upon force or temperature stimuli was obtained through a developed electronic circuit. Due to the material resistive variation, the sensors are excited by a continuous potential of 3.3 V and the readout of the response was based on a Wheatstone bridge [61]. A multiplexer (Texas Instruments® CD74HCT4067M) allows each sensor from a given matrix to be read in the Wheatstone bridge, which is composed by a reference resistor provided by a digital potentiometer (Texas Instruments® TPL0501) in series with the sensor being measured and a 12-bit Digital-to-Analog converter (DAC) (Microchip® MCP48FEB21) that provides the reference calibrated voltage to be compared in the operational amplifier (Microchip® MCP6201) before being measured by the 10-bit Analog-to-Digital converter (ADC) present in the 32-bit microcontroller (Microchip® PIC32MX230F128L). The system works by applying an initial calibration in order to access the response without stimuli at system startup. Further, the calibrated data stored in the memory is used and subtracted using the voltage provided by the DAC, to obtain a near-zero response for the no stimuli case. Furthermore, the sensor measured data are acquired and communicated by USB-serial chip converter (FTDI® FT232RL) and treated by a C++ application developed in Qt Creator environment, using open-source library qCustomPlot, in order to output custom developed graphs for multi-plotting of several sensors simultaneously.

The piezoresistive and thermoresistive performance of the 20G/BW composites is illustrated in Figure 6. The 3D designed pattern with 4 columns works as individual sensors when the force is applied pressing the fingers over each column. In Figure 6A it can be observed the simultaneous stimulus in sensor 1 and 2, and individual stimulus in sensor 3 and 4. The piezoresistive response of the 20G/BW composite when a force is

applied on the corresponding sensors is identified in the graphics, the time to relax to the original deformation being indicative of the viscoelastic properties of wax [62]. The applied force, in related materials, corresponds to 1 N and 2 μm of strain [28]. The resistance changes are at least 20 Ω in sensors with initial resistance of 200 Ω.

The thermoresistive response of the bottom surface of the device presents the correlation between resistance values and temperature variations (Figure 6B) during heating from 22 to 60 ºC using a hotplate and cooling from 22 to 0 ºC using ice, represented by a red and blue zone in Figure 6B, respectively. The resistance changes near 10 Ω, being the initial resistance of about 240 Ω.

Therefore, it was demonstrated that natural beeswax reinforced with graphene can be processed by additive manufacturing in specific patterns for practical applications with simple readout electronic systems due to large resistance variations upon external mechanical or thermal variation.

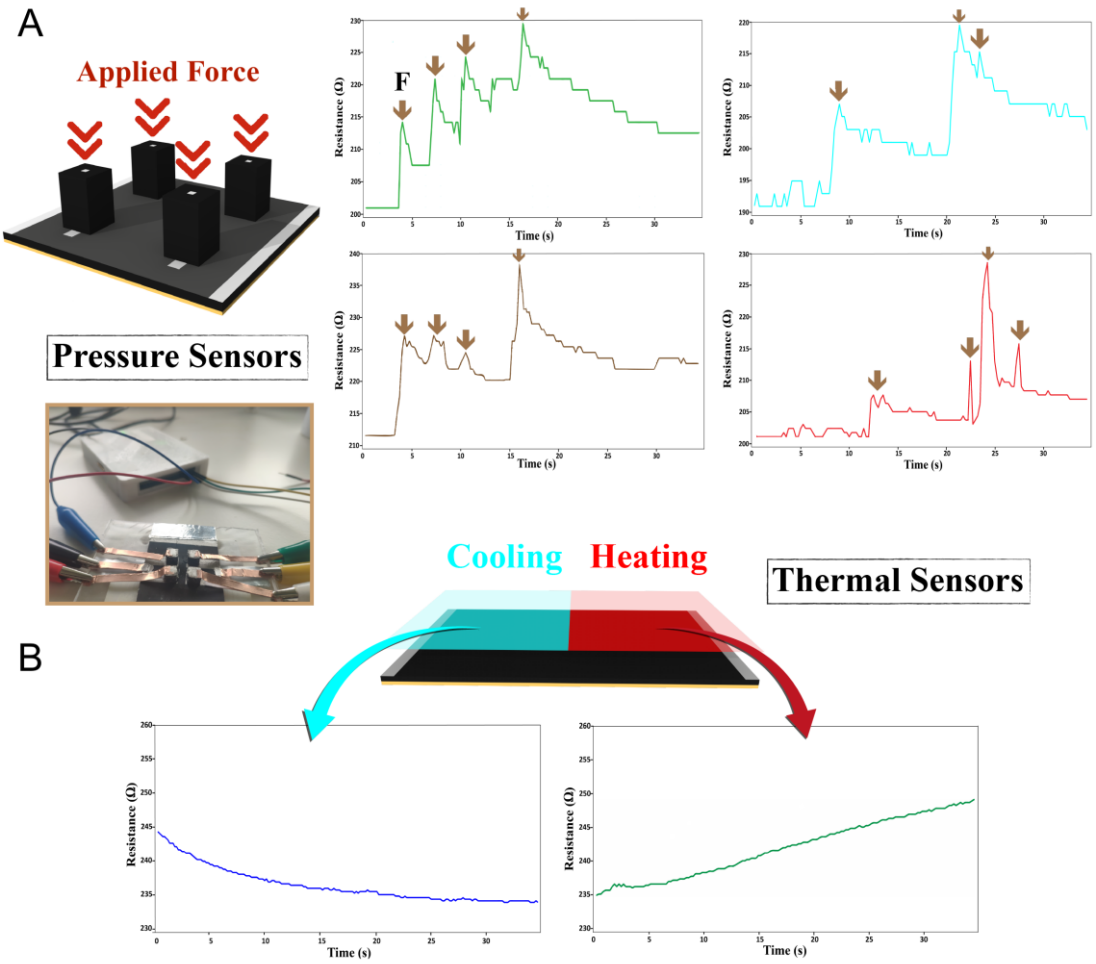

Figure 6- Multifunctional sensing performance of beeswax reinforced with 20 wt.% of graphene processed by additive manufacturing: 3D printed columns for piezoresistive force sensors (A) and screen-printed bottom layer for thermoresistive sensing (B).

3.3. Functional thermal healing

Beeswax is characterized by its low melting temperature (≈60 ºC [63]) and its hydrophobicity [15, 39]. The properties of low temperature phase changing materials such as natural waxes can be used for the development of thermal-healing devices, depending on the wax type or reinforcing material content [64, 65], allowing to recover the functional electrical and sensing properties after the healing process.

The graphene/beeswax composites developed in the present work show excellent functional piezoresistive and thermoresistive response than can be recovered upon device fracture though a thermal-healing process, as demonstrated in Figure 7A and B. Screen-printed 20G/BW composites, with tri-fork structure, over Kapton and paper (smooth and porous substrates, respectively) where submitted to single or multiple cuts between 100 to 150 μm of width (Figure 7C and D) perpendicularly to the orientation of the films, with

the consequent increase of the electrical resistance of the patterns. Then the composites were placed in an oven (Linkam THMSE 600), a specific thermal program was applied while the electrical resistance was measured simultaneously. The thermal program consists of heating the composite near to the melting temperature (changing from solid to liquid state of the beeswax composite), starting by 10 min at 60 ºC and then at 70 ºC and observing in real-time the electrical resistance variation of the cut materials during the heating process. For composite printed over paper (Figure 7B), an initial heating at 50 ºC during 10 min was performed without significant decrease of the electrical resistance.

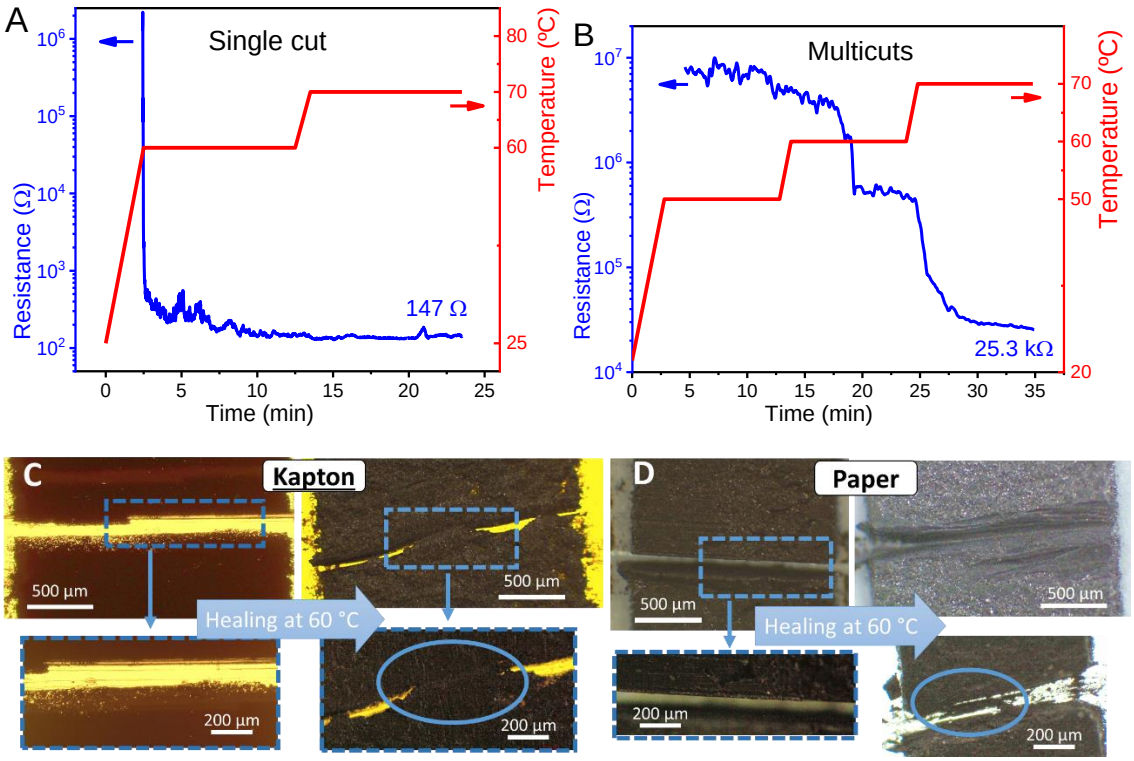

Figure 7- Thermal-healing characteristics of the 20G/BW composites with (A) a single and (B) multiple cuts, respectively, on screen-printed samples on (C) Kapton and (D) paper substrates. The samples were heated for 10 min at 50, 60 and 70 ºC.

The 20G/BW composite demonstrates the thermal healing characteristics of the material, with the healing process occurring at 60 ºC, in printed samples, independently of the substrate although with distinct characteristics. Indeed, the thermal healing process of the composite is faster in the Kapton substrate (Figure 7A and C), where during the first minute at 60 ºC the separated parts of the film reassemble more rapidly, and the electrical conductivity is restored. It is to notice that the recovered electrical resistance is close to

the initial value (80 Ω initial resistance vs. 147 Ω after healing), for a single cut of the conductive tracks on Kapton substrate. This performance is similar for multiple (3 cuts) for the same composite in the same substrate. Printed composites on paper (Figure 7D) show a different response: the porosity and fibrillar structure of the paper, which holds the wax in the pores structure, makes it more difficult for the wax to diffuse at the melting temperature and, therefore, the printed pattern on paper takes more time to regenerate and the electrical conductivity is two orders of magnitude (25.3 kΩ) higher that the initial resistance (≈130 Ω) for the printed composite with 3 cuts. Comparable electrical and thermal performance was found for the composite with just one cut for the printed tracks on paper substrate.

3.4. Proof-of-concept for thermal healing

To demonstrate the electrical conductivity of the composites and the thermal- healing characteristics, a proof-of-concept device was developed (Figure 8). The 20G/BW composite was screen-printed in a tri-forked-shape on Kapton and paper (Figure 8A) and a LED was connected to each tine. One commercial battery (1.5 V) was used to power the LEDs.

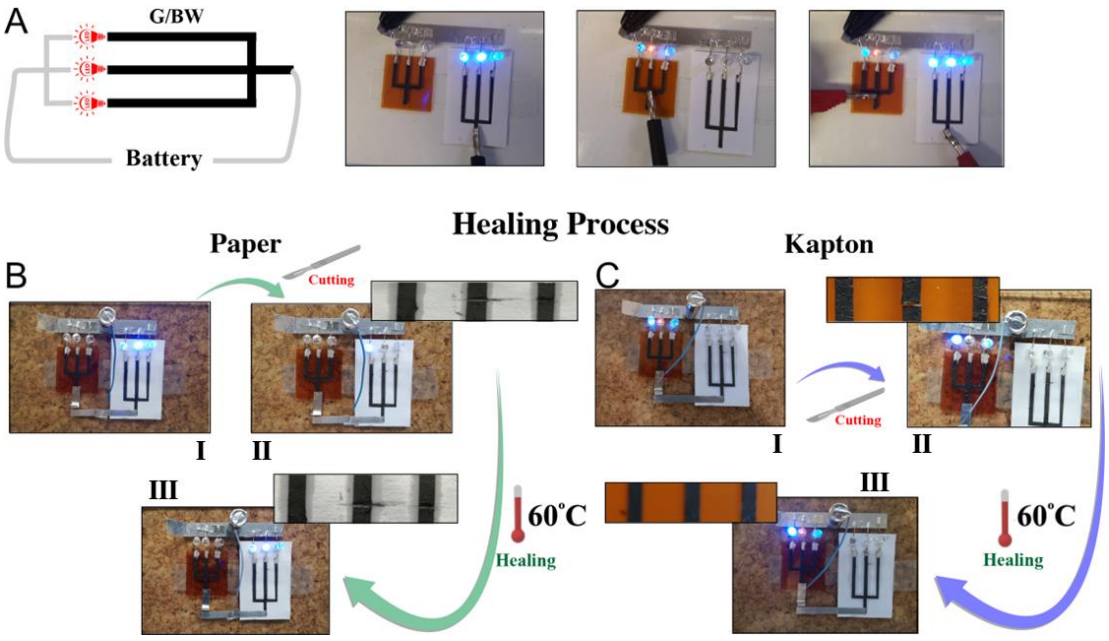

Figure 8- Illustrative device developed with the 20G/BW composite printed on Kapton and paper substrates. The conductive patters are shaped like a fork with 3 tines A) to light LEDs. Functional thermal healing using a single cut in the middle tine of each sensor and heated at 60 ºC for 10 min on B) Paper and at 60 ºC for 10 min on C) Kapton.

A single cut was applied to the middle tine of the tri-fork patterns (step II in Figure 8B for paper and Figure 8C for Kapton) leads to interruption of the current to the middle LED, which is regenerated (step III in Figure 8B and C) after thermal-healing at 60 ºC on Kapton and at 60 ºC on paper.

3.5. Recyclability and reuse of the multifunctional beeswax composites

Finally, the recyclability and reuse of the printed 20G/BW composites was evaluated. Screen-printed composites over Kapton were removed to a laboratory watch glass and heated at 60 ºC (Figure 9I to III). After that, the beeswax composite was first printed and then re-printed with two distinct patterns presenting electrical resistance values of 93 and 266 Ω, by volume and surface methods. The initial resistance is about 45 and 140 Ω, in volume and surface, respectively, increasing near 2 times in the recycled and reused samples. This demonstration proves that in addition to the reutilization of the functional beeswax and its several reuses and printing possibilities on different substrates, it can also be reprinted on the same substrate, modifying the geometry for specific applications.

Figure 9- Recycling and reuse of the beeswax after screen-printing (I) over Kapton, then removed (II-III) and (IV-V) and heated at 60 ºC for 10 min, showing low resistance values for pattern lines.

Conclusions

Multifunctional sensing characteristics, thermal healing, recyclability and reuse of natural beeswax reinforced with graphene were evaluated in materials processed by solvent-free additive manufacturing. Beeswax and its composites present a melting temperature of 60 ºC, hydrophobic and non-cytotoxic characteristics. Composites show an excellent electrical conductivity of 50 S/m and a piezoresistive sensibility of $GF \approx 10$, the value being among the best achieved for piezoresistive natural-base composite, and a thermoresistive sensibility of 120 %/ºC in the temperature range from 25 to 50 ºC.

Besides being highly conductive, the composite show low-temperature regeneration properties, the functional electrical conductivity of printed patters being recovered after single and multiple cults in proof-of-concept devices upon heating at 60 ºC.

Finally, these composites can be recycled and reused without losing functional characteristics, by a simple thermal process. The excellent functional characteristics, compatibility with solvent-free additive manufacturing technologies, and the proof-of-concept devices demonstrate the suitably of beeswax and beeswax composites for next generation environmentally friendly functional materials for sustainable sensing.

Acknowledgments

This work was supported by the Portuguese Foundation for Science and Technology (FCT) for financial support under strategic funding UID/FIS/04650/2021 and UIDB/00319/2020. The authors also thank the FCT for financial support under grant SFRH/BD/140698/2018 (R.B.P.), 2020.04163.CEECIND (C.R) and SFRH/BDP/110914/2015 (P.C). The authors acknowledge funding by Spanish State Research Agency (AEI) and the European Regional Development Fund (ERFD) through the project PID2019-106099RB-C43/AEI/10.13039/501100011033 and from the Basque Government Industry Departments under the ELKARTEK program. Technical and human support provided by SGIker (UPV/EHU, MICINN, GV/EJ, EGEF and ESF) is gratefully acknowledged.

References

[1] Y. Hu, Recent progress in field-assisted additive manufacturing: materials, methodologies, and applications, Materials Horizons 8(3) (2021) 885-911. https://doi.org/10.1039/D0MH01322F.
[2] C.M. Costa, M.M. Silva, S. Lanceros-Méndez, Battery separators based on vinylidene fluoride (VDF) polymers and copolymers for lithium ion battery applications, RSC Advances 3(29) (2013) 11404-11417. https://doi.org/10.1039/C3RA40732B.
[3] S. Bose, C. Koski, A.A. Vu, Additive manufacturing of natural biopolymers and composites for bone tissue engineering, Materials Horizons 7(8) (2020) 2011-2027. https://doi.org/10.1039/D0MH00277A.
[4] J.R. Dios, C. Garcia-Astrain, S. Gonçalves, P. Costa, S. Lanceros-Méndez, Piezoresistive performance of polymer-based materials as a function of the matrix and nanofiller content to walking detection application, Composites Science and Technology 181 (2019) 107678. https://doi.org/https://doi.org/10.1016/j.compscitech.2019.107678.
[5] P. Costa, M.F. Carvalho, V. Correia, J.C. Viana, S. Lanceros-Mendez, Polymer Nanocomposite-Based Strain Sensors with Tailored Processability and Improved Device Integration, ACS Applied Nano Materials 1(6) (2018) 3015-3025. https://doi.org/10.1021/acsanm.8b00647.
[6] W. Huang, H. Li, L. Zheng, X. Lai, H. Guan, Y. Wei, H. Feng, X. Zeng, Superhydrophobic and high-performance wood-based piezoresistive pressure sensors for detecting human motions, Chemical Engineering Journal 426 (2021) 130837. https://doi.org/https://doi.org/10.1016/j.cej.2021.130837.
[7] V. Flaris, G. Singh, Recent developments in biopolymers, Journal of Vinyl and Additive Technology 15(1) (2009) 1-11. https://doi.org/https://doi.org/10.1002/vnl.20171.
[8] A. Chamas, H. Moon, J. Zheng, Y. Qiu, T. Tabassum, J.H. Jang, M. Abu-Omar, S.L. Scott, S. Suh, Degradation Rates of Plastics in the Environment, ACS Sustainable Chemistry & Engineering 8(9) (2020) 3494-3511. https://doi.org/10.1021/acssuschemeng.9b06635.
[9] R. Kumar, A. Verma, A. Shome, R. Sinha, S. Sinha, P.K. Jha, R. Kumar, P. Kumar, Shubham, S. Das, P. Sharma, P.V. Vara Prasad, Impacts of Plastic Pollution on Ecosystem Services, Sustainable Development Goals, and Need to Focus on Circular Economy and Policy Interventions, Sustainability 13(17) (2021) 9963.
[10] M.U. Bukhari, A. Khan, K.Q. Maqbool, A. Arshad, K. Riaz, A. Bermak, Waste to energy: Facile, low-cost and environment-friendly triboelectric nanogenerators using recycled plastic and electronic wastes for self-powered portable electronics, Energy Reports 8 (2022) 1687-1695. https://doi.org/https://doi.org/10.1016/j.egyr.2021.12.072.
[11] R. Rajesh, D. Kanakadhurga, N. Prabaharan, Electronic waste: A critical assessment on the unimaginable growing pollutant, legislations and environmental impacts, Environmental Challenges 7 (2022) 100507. https://doi.org/https://doi.org/10.1016/j.envc.2022.100507.
[12] R. Hatti-Kaul, L.J. Nilsson, B. Zhang, N. Rehnberg, S. Lundmark, Designing Biobased Recyclable Polymers for Plastics, Trends in Biotechnology 38(1) (2020) 50-67. https://doi.org/https://doi.org/10.1016/j.tibtech.2019.04.011.
[13] G.o.t.U.S.o. America, Executive Order on Catalyzing Clean Energy Industries and Jobs Through Federal Sustainability, 2021. https://www.whitehouse.gov/briefing-room/presidential-actions/2021/12/08/executive-order-on-catalyzing-clean-energy-industries-and-jobs-through-federal-sustainability/?utm_source=link.
[14] C. Zhang, J. Xue, X. Yang, Y. Ke, R. Ou, Y. Wang, S.A. Madbouly, Q. Wang, From plant phenols to novel bio-based polymers, Progress in Polymer Science 125 (2022) 101473. https://doi.org/https://doi.org/10.1016/j.progpolymsci.2021.101473.
[15] Z. Liu, X. Zhu, Y. Tian, K. Zhou, J. Cheng, J. Zhang, Bio-based recyclable Form-Stable phase change material based on thermally reversible Diels–Alder reaction for sustainable thermal energy storage, Chemical Engineering Journal 448 (2022) 137749. https://doi.org/https://doi.org/10.1016/j.cej.2022.137749.

[16] S.K. Kumaran, M. Chopra, E. Oh, H.-J. Choi, Chapter 11 - Biopolymers and natural polymers, in: R. Narain (Ed.), Polymer Science and Nanotechnology, Elsevier2020, pp. 245-256. https://doi.org/https://doi.org/10.1016/B978-0-12-816806-6.00011-X.
[17] I.B. Basumatary, A. Mukherjee, V. Katiyar, S. Kumar, Biopolymer-based nanocomposite films and coatings: recent advances in shelf-life improvement of fruits and vegetables, Critical Reviews in Food Science and Nutrition (2020) 1-24. https://doi.org/10.1080/10408398.2020.1848789.
[18] P. Gupta, K.K. Nayak, Characteristics of protein-based biopolymer and its application, Polymer Engineering & Science 55(3) (2015) 485-498. https://doi.org/https://doi.org/10.1002/pen.23928.
[19] Y. Zhang, J. Bi, S. Wang, Q. Cao, Y. Li, J. Zhou, B.-W. Zhu, Functional food packaging for reducing residual liquid food: Thermo-resistant edible super-hydrophobic coating from coffee and beeswax, Journal of Colloid and Interface Science 533 (2019) 742-749. https://doi.org/https://doi.org/10.1016/j.jcis.2018.09.011.
[20] W. Zhang, H. Xiao, L. Qian, Beeswax–chitosan emulsion coated paper with enhanced water vapor barrier efficiency, Applied Surface Science 300 (2014) 80-85. https://doi.org/https://doi.org/10.1016/j.apsusc.2014.02.005.
[21] H. Tian, K. Wang, H. Lan, Y. Wang, Z. Hu, L. Zhao, Effect of hybrid gelator systems of beeswax-carrageenan-xanthan on rheological properties and printability of litchi inks for 3D food printing, Food Hydrocolloids 113 (2021) 106482. https://doi.org/https://doi.org/10.1016/j.foodhyd.2020.106482.
[22] M. Murcia Morales, M.J. Gómez Ramos, P. Parrilla Vázquez, F.J. Díaz Galiano, M. García Valverde, V. Gámiz López, J. Manuel Flores, A.R. Fernández-Alba, Distribution of chemical residues in the beehive compartments and their transfer to the honeybee brood, Science of The Total Environment 710 (2020) 136288. https://doi.org/https://doi.org/10.1016/j.scitotenv.2019.136288.
[23] S.M. Won, J. Koo, K.E. Crawford, A.D. Mickle, Y. Xue, S. Min, L.A. McIlvried, Y. Yan, S.B. Kim, S.M. Lee, B.H. Kim, H. Jang, M.R. MacEwan, Y. Huang, R.W. Gereau IV, J.A. Rogers, Natural Wax for Transient Electronics, Advanced Functional Materials 28(32) (2018) 1801819. https://doi.org/https://doi.org/10.1002/adfm.201801819.
[24] A. Roy, C.K. Maity, Nanostructured 2D Materials for Biomedical, Nano Bioengineering, and Nanomechanical Devices, in: S. Singh, K. Verma, C. Prakash (Eds.), Advanced Applications of 2D Nanostructures: Emerging Research and Opportunities, Springer Singapore, Singapore, 2021, pp. 211-229. https://doi.org/10.1007/978-981-16-3322-5_11.
[25] K. Ke, L. Yue, H. Shao, M.-B. Yang, W. Yang, I. Manas-Zloczower, Boosting electrical and piezoresistive properties of polymer nanocomposites via hybrid carbon fillers: A review, Carbon 173 (2021) 1020-1040. https://doi.org/https://doi.org/10.1016/j.carbon.2020.11.070.
[26] M. Franco, A. Motealleh, C.M. Costa, L. Hilliou, N. Perinka, C. Ribeiro, J.C. Viana, P. Costa, S. Lanceros-Mendez, Environmentally Friendly Conductive Screen-Printable Inks Based on N-Doped Graphene and Polyvinylpyrrolidone, Advanced Engineering Materials 24(6) (2022) 2101258. https://doi.org/https://doi.org/10.1002/adem.202101258.
[27] V.S. Saji, Wax-based artificial superhydrophobic surfaces and coatings, Colloids and Surfaces A: Physicochemical and Engineering Aspects 602 (2020) 125132. https://doi.org/https://doi.org/10.1016/j.colsurfa.2020.125132.
[28] R. Brito-Pereira, C.R. Tubio, P. Costa, S. Lanceros-Mendez, Multifunctional wax based conductive and piezoresistive nanocomposites for sensing applications, Composites Science and Technology 213 (2021) 108892. https://doi.org/https://doi.org/10.1016/j.compscitech.2021.108892.
[29] M. Liu, C. Zhang, F. Liu, Understanding wax screen-printing: A novel patterning process for microfluidic cloth-based analytical devices, Analytica Chimica Acta 891 (2015) 234-246. https://doi.org/https://doi.org/10.1016/j.aca.2015.06.034.

[30] L. Arboleda, A. Ares, M.J. Abad, A. Ferreira, P. Costa, S. Lanceros-Mendez, Piezoresistive response of carbon nanotubes-polyamides composites processed by extrusion, Journal of Polymer Research 20(12) (2013) 326. https://doi.org/10.1007/s10965-013-0326-y.
[31] J. Vicente, P. Costa, S. Lanceros-Mendez, J.M. Abete, A. Iturrospe, Electromechanical Properties of PVDF-Based Polymers Reinforced with Nanocarbonaceous Fillers for Pressure Sensing Applications, Materials 12(21) (2019) 3545.
[32] A. Mann, C.M. Bürgel, P. Groche, A Modeling Strategy for Predicting the Properties of Paraffin Wax Actuators, Actuators 7(4) (2018) 81.
[33] A. Ferreira, M. Martínez, A. Ansón-Casaos, L. Gómez-Pineda, F. Vaz, S. Lanceros-Mendez, Relationship between electromechanical response and percolation threshold in carbon nanotube/poly (vinylidene fluoride) composites, Carbon 61 (2013) 568-576.
[34] R. Wu, L. Ma, C. Hou, Z. Meng, W. Guo, W. Yu, R. Yu, F. Hu, X.Y. Liu, Silk Composite Electronic Textile Sensor for High Space Precision 2D Combo Temperature–Pressure Sensing, Small 15(31) (2019) 1901558. https://doi.org/https://doi.org/10.1002/smll.201901558.
[35] S. Gupta, J. Ivvala, H.S. Grewal, Development of natural wax based durable superhydrophobic coatings, Industrial Crops and Products 171 (2021) 113871. https://doi.org/https://doi.org/10.1016/j.indcrop.2021.113871.
[36] S.N.M. Jayapal, V.K. Dubey, S. Dinesh, A. Wahab, A. Abdul Khaleel, P.N. Kadiresh, Thermal stability and kinetic study of blended Beeswax-ethylene vinyl acetate based hybrid rocket fuels, Thermochimica Acta 702 (2021) 178989. https://doi.org/https://doi.org/10.1016/j.tca.2021.178989.
[37] K. Niu, K. Song, Hot waxing treatment improves the aging resistance of wood surface under UV radiation and water, Progress in Organic Coatings 161 (2021) 106468. https://doi.org/https://doi.org/10.1016/j.porgcoat.2021.106468.
[38] E. Carrilho, A.W. Martinez, G.M. Whitesides, Understanding wax printing: a simple micropatterning process for paper-based microfluidics, Analytical chemistry 81(16) (2009) 7091-7095.
[39] S. Naderizadeh, J.A. Heredia-Guerrero, G. Caputo, S. Grasselli, A. Malchiodi, A. Athanassiou, I.S. Bayer, Superhydrophobic Coatings from Beeswax-in-Water Emulsions with Latent Heat Storage Capability, Advanced Materials Interfaces 6(5) (2019) 1801782.
[40] L. Svečnjak, G. Baranović, M. Vinceković, S. Prđun, D. Bubalo, I.T. Gajger, An Approach for Routine Analytical Detection of Beeswax Adulteration Using FTIR-ATR Spectroscopy, Journal of Apicultural Science 59(2) (2015) 37-49. https://doi.org/doi:10.1515/jas-2015-0018.
[41] Z.N. Diyana, R. Jumaidin, M.Z. Selamat, M.S.M. Suan, Thermoplastic starch/beeswax blend: Characterization on thermal mechanical and moisture absorption properties, International Journal of Biological Macromolecules 190 (2021) 224-232. https://doi.org/https://doi.org/10.1016/j.ijbiomac.2021.08.201.
[42] M. Amin, N. Putra, E.A. Kosasih, E. Prawiro, R.A. Luanto, T.M.I. Mahlia, Thermal properties of beeswax/graphene phase change material as energy storage for building applications, Applied Thermal Engineering 112 (2017) 273-280. https://doi.org/https://doi.org/10.1016/j.applthermaleng.2016.10.085.
[43] R. C. R, S.P. Sundaran, J. A, S. Athiyanathil, Fabrication of superhydrophobic polycaprolactone/beeswax electrospun membranes for high-efficiency oil/water separation, RSC Advances 7(4) (2017) 2092-2102. https://doi.org/10.1039/C6RA26123J.
[44] X. Wu, C. Lu, X. Zhang, Z. Zhou, Conductive natural rubber/carbon black nanocomposites via cellulose nanowhisker templated assembly: tailored hierarchical structure leading to synergistic property enhancements, Journal of Materials Chemistry A 3(25) (2015) 13317-13323.
[45] M.a.A. Tarawneh, S.A. Saraireh, R.S. Chen, S.H. Ahmad, M.A.M. Al-Tarawni, M. Al-Tweissi, L.J. Yu, Mechanical, thermal, and conductivity performances of novel thermoplastic natural rubber/graphene nanoplates/polyaniline composites, Journal of Applied Polymer Science 137(28) (2020) 48873.

[46] F.A. Oliveira, N. Alves, J.A. Giacometti, C.J. Constantino, L.H. Mattoso, A.M. Balan, A.E. Job, Study of the thermomechanical and electrical properties of conducting composites containing natural rubber and carbon black, Journal of applied polymer science 106(2) (2007) 1001-1006.
[47] N.D. Luong, N. Pahimanolis, U. Hippi, J.T. Korhonen, J. Ruokolainen, L.-S. Johansson, J.-D. Nam, J. Seppälä, Graphene/cellulose nanocomposite paper with high electrical and mechanical performances, Journal of Materials Chemistry 21(36) (2011) 13991-13998.
[48] L. Zuo, F. Zhang, B. Gao, B. Zuo, Fabrication of electrical conductivity and reinforced electrospun silk nanofibers with MWNTs, Fibres & Textiles in Eastern Europe (2017).
[49] J.C. Soares, T.C.B. Pereira, K.M. Costa, T. Maraschin, N.R. Basso, M.R. Bogo, Developmental neurotoxic effects of graphene oxide exposure in zebrafish larvae (Danio rerio), Colloids and Surfaces B: Biointerfaces 157 (2017) 335-346. https://doi.org/https://doi.org/10.1016/j.colsurfb.2017.05.078.
[50] P.S. Das, S.H. Park, K.Y. Baik, J.W. Lee, J.Y. Park, Thermally reduced graphene oxide-nylon membrane based epidermal sensor using vacuum filtration for wearable electrophysiological signals and human motion monitoring, Carbon 158 (2020) 386-393. https://doi.org/https://doi.org/10.1016/j.carbon.2019.11.001.
[51] L. Horta Romarís, M.V. González Rodríguez, B. Huang, P. Costa, A. Lasagabáster Latorre, S. Lanceros-Mendez, M.J. Abad López, Multifunctional electromechanical and thermoelectric polyaniline–poly(vinyl acetate) latex composites for wearable devices, Journal of Materials Chemistry C 6(31) (2018) 8502-8512. https://doi.org/10.1039/C8TC02327A.
[52] W.-G. La, S. Park, H.-H. Yoon, G.-J. Jeong, T.-J. Lee, S.H. Bhang, J.Y. Han, K. Char, B.-S. Kim, Delivery of a Therapeutic Protein for Bone Regeneration from a Substrate Coated with Graphene Oxide, Small 9(23) (2013) 4051-4060. https://doi.org/https://doi.org/10.1002/smll.201300571.
[53] C. Yan, J. Wang, W. Kang, M. Cui, X. Wang, C.Y. Foo, K.J. Chee, P.S. Lee, Highly Stretchable Piezoresistive Graphene–Nanocellulose Nanopaper for Strain Sensors, Advanced Materials 26(13) (2014) 2022-2027. https://doi.org/https://doi.org/10.1002/adma.201304742.
[54] Y. Li, G. Liu, L. Wang, J. Zhang, M. Xu, S.Q. Shi, Multifunctional conductive graphite/cellulosic microfiber-natural rubber composite sponge with ultrasensitive collision-warning and fire-waring, Chemical Engineering Journal 431 (2022) 134046. https://doi.org/https://doi.org/10.1016/j.cej.2021.134046.
[55] M. Franco, R. Alves, N. Perinka, C. Tubio, P. Costa, S. Lanceros-Mendéz, Water-Based Graphene Inks for All-Printed Temperature and Deformation Sensors, ACS Applied Electronic Materials 2(9) (2020) 2857-2867. https://doi.org/10.1021/acsaelm.0c00508.
[56] L. Duan, D.R. D'Hooge, L. Cardon, Recent progress on flexible and stretchable piezoresistive strain sensors: From design to application, Progress in Materials Science 114 (2020) 100617. https://doi.org/https://doi.org/10.1016/j.pmatsci.2019.100617.
[57] F. Avilés, A.I. Oliva-Avilés, M. Cen-Puc, Piezoresistivity, Strain, and Damage Self-Sensing of Polymer Composites Filled with Carbon Nanostructures, Advanced Engineering Materials 20(7) (2018) 1701159. https://doi.org/https://doi.org/10.1002/adem.201701159.
[58] K.J. Groh, T. Backhaus, B. Carney-Almroth, B. Geueke, P.A. Inostroza, A. Lennquist, H.A. Leslie, M. Maffini, D. Slunge, L. Trasande, A.M. Warhurst, J. Muncke, Overview of known plastic packaging-associated chemicals and their hazards, Science of The Total Environment 651 (2019) 3253-3268. https://doi.org/https://doi.org/10.1016/j.scitotenv.2018.10.015.
[59] J. Yang, D. Wei, L. Tang, X. Song, W. Luo, J. Chu, T. Gao, H. Shi, C. Du, Wearable temperature sensor based on graphene nanowalls, RSC Advances 5(32) (2015) 25609-25615. https://doi.org/10.1039/C5RA00871A.
[60] K.L. Lasater, E.T. Thostenson, In situ thermoresistive characterization of multifunctional composites of carbon nanotubes, Polymer 53(23) (2012) 5367-5374. https://doi.org/https://doi.org/10.1016/j.polymer.2012.09.022.
[61] P. Costa, J.R. Dios, J. Cardoso, J.J. Campo, C.R. Tubio, B.F. Gon alves, N. Castro, S. Lanceros-Méndez, Polycarbonate based multifunctional self-sensing 2D and 3D printed structures for

aeronautic applications, Smart Materials and Structures 30(8) (2021). https://doi.org/10.1088/1361-665X/ac0cbe.
[62] T.H. Shellhammer, T.R. Rumsey, J.M. Krochta, Viscoelastic properties of edible lipids, Journal of Food Engineering 33(3) (1997) 305-320. https://doi.org/https://doi.org/10.1016/S0260-8774(97)00030-7.
[63] C. Zhang, Y. Ma, K. Guo, X. Zhao, High-Pressure Homogenization Lowers Water Vapor Permeability of Soybean Protein Isolate–Beeswax Films, Journal of Agricultural and Food Chemistry 60(9) (2012) 2219-2223. https://doi.org/10.1021/jf2035109.
[64] Y. Wang, Y. Liu, J. Li, L. Chen, S. Huang, X. Tian, Fast self-healing superhydrophobic surfaces enabled by biomimetic wax regeneration, Chemical Engineering Journal 390 (2020) 124311. https://doi.org/https://doi.org/10.1016/j.cej.2020.124311.
[65] H.-l. Li, S.-n. Xiao, H.-l. Yu, Y.-h. Xue, J.-h. Yang, A review of graphene-based films for heat dissipation, New Carbon Materials 36(5) (2021) 897-908. https://doi.org/https://doi.org/10.1016/S1872-5805(21)60092-6.

Table of Contents

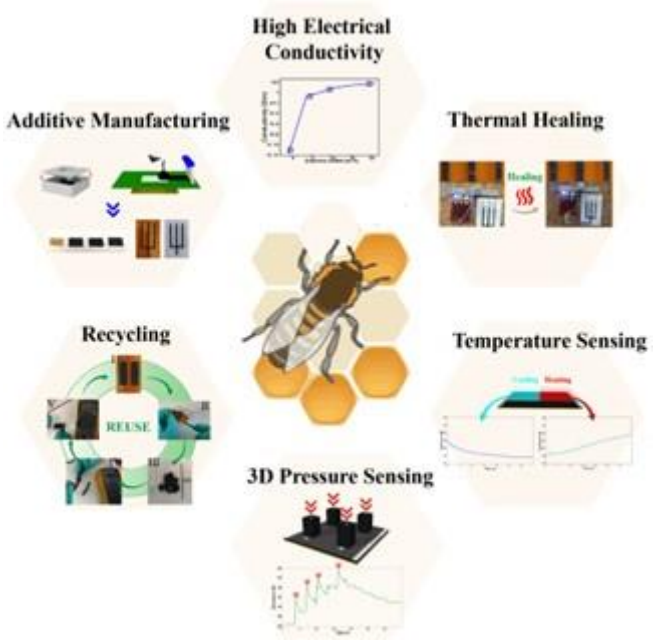
High Electrical Conductivity
Additive Manufacturing
Thermal Healing
Recycling
REUSE
Temperature Sensing
3D Pressure Sensing